SUPPLEMENTARY INFORMATION

Targeting an N-terminal Acetylation Dependent Protein Interaction

Daniel C. Scott[1,2,10], Jared T. Hammill[3,4,10], Jaeki Min[3], David Y. Rhee[5], Michele Connelly[3], Vladislav O. Sviderskiy[1], Deepak Bhasin[3], Yizhe Chen[3,4], Su-Sien Ong[3], Sergio C. Chai[3], Asli N. Goktug[3], Guochang Huang[6], Julie K. Monda[1], Jonathan Low[3], Ho Shin Kim[3,4], Joao A. Paulo[5], Joe R. Cannon[5], Anang A. Shelat[3], Taosheng Chen[3], Ian R. Kelsall[7], Arno F. Alpi[8], Vishwajeeth Pagala[9], Xusheng Wang[9], Junmin Peng[1,9], Bhuvanesh Singh[6], J. Wade Harper[5], Brenda A. Schulman[1,2,11], R. Kip Guy[3,4,11]

[1] Department of Structural Biology, St. Jude Children's Research Hospital, Memphis, TN 38105

[2] Howard Hughes Medical Institute, St. Jude Children's Research Hospital, Memphis, TN 38105

[3] Department of Chemical Biology and Therapeutics, St. Jude Children's Research Hospital, Memphis, TN 38105

[4] Present address: Department of Pharmaceutical Sciences, University of Kentucky, Lexington, KY 40508

[5] Department of Cell Biology, Harvard Medical School, Boston, MA 02115

[6] Laboratory of Epithelial Cancer Biology, Memorial Sloan-Kettering Cancer Center, New York, NY 10021

[7] MRC Protein Phosphorylation and Ubiquitylation Unit, University of Dundee, Dundee, UK

[8] Department of Molecular Machines and Signaling, Max Planck Institute of Biochemistry, Martinsried, Germany

[9] St. Jude Proteomics Facility, St. Jude Children's Research Hospital, Memphis, TN 38105

[10] Co-first author

[11] Co-corresponding author

[11] Correspondence: Brenda.Schulman@stjude.org and kip.guy@uky.edu

Supplementary Results

Supplementary Table 1. Small molecule screening data

Category	Parameter	Description
Assay	Type of assay	Biochemical ligand competition assay
	Target	DCN1 (aka DCUN1D1)
	Primary measurement	Detection of the Time-Resolved Fluoresce Resonance Energy Transfer (TR-FRET) signal between a biotinylated version of DCN1 (PONY domain alone), recognized by terbium-linked streptavidin, and a stapled peptide corresponding to N-terminally acetylated UBE2M labeled at its C-terminus with AlexaFluor 488.
	Key reagents	Biotinylated version of DCN1 (PONY domain alone); commercial terbium-linked streptavidin (ThermoFisher, PV3965); hydrocarbon stapled Acetyl-UBE2M$^{1-12}$ peptide (sequence Acetyl-MIKLZ*SLKZ*QKKC, where Z* is 2,4'-pentenylalanine closed after synthesis to create the hydrocarbon staple) labeled at its C-terminus with AlexaFluor 488.
	Assay protocol	See online methods "TR-FRET Assay and HTS Campaign"
	Additional comments	More details are provided in the supplementary information
Library	Library size	601,194
	Library composition	The current St. Jude Children's Research Hospital (SJCRH) department of Chemical Biology and Therapeutics (CBT) chemical library consists of roughly 600,000 unique molecules purchased from a variety of commercial sources. The library can be subdivided into 4 categories: approved drugs (~ 1,100 compounds); other known bioactives (~ 2,500 compounds); focused sets directed at defined targets including GPCR's, kinases, proteases, and phosphatases (~ 45,000 compounds), and the diversity collection. For more information regarding the selection of library members please see: Shelat, A. A.; Guy, R. K. Scaffold composition and biological relevance of screening libraries. *Nat Chem Biol* **2007,** *3* (8), 442-446
	Source	
	Additional comments	
Screen	Format	384-well microtiter plates
	Concentration(s) tested	30 µM, 0.1% DMSO (final assay concentration)
	Plate controls	Each assay plate contained 6 replicates of positive and negative controls. High signal: unlabeled UBE2M peptide; Low signal: DMSO
	Reagent/ compound dispensing system	The HTS was implemented on a fully-automated system (HighRes Biosolutions) with an integrated robotic arm (Staübli). The protein and peptide master mixture was kept chilled at 4 °C, and dispensed into solid black 384-well assay plates (20 µL/well) using Matrix Wellmate bulk dispensers (ThermoFisher), followed by centrifugation using a V-Spin plate centrifuge (Agilent Technologies). Test articles and controls (stored as 10 mM solutions in DMSO donor plates) were transferred to the assay plates using a pintool (V&P Scientific) equipped with FP1S50 pins resulting in final compound concentrations of 30 µM.
	Detection instrument and software	The TR-FRET signal with a PHERAstar FS plate reader (BMG Labtech) equipped with modules for

		excitation at 337 nm and emissions at 490 and 520 nm. The integration start was set to 100 µs and the integration time to 200 µs. The number of flashes was fixed at 100. The ratio of 520/490 was used as TR-FRET signal in calculations.
	Assay validation/QC	The assay validation was carried out over three days during which three separate plates containing different layouts of the high, medium and low controls (i.e. plate 1, plate 2 and plate 3) were each run in triplicate. The screen performance was robust and highly reproducible with an average signal window of 9.8 and an average Z' factor of 0.7. The primary screen gave an average final Z'-prime of 0.56
	Correction factors	
	Normalization	Assay endpoints were normalized from 0% (DMSO only) to 100% inhibition (unlabeled competitor peptide) for hit selection and for curve fitting
	Additional comments	
Post-HTS analysis	Hit criteria	Based on receiver operating characteristic (ROC) analysis, a cut-off value of > 45% inhibition was selected, which included approximately 80% of all true positives and a false positive rate of 20%.
	Hit rate	856 active hits (0.15% hit rate)
	Additional assay(s)	IC_{50} values were determined for each hit using a 10-point dose-response with concentrations ranging from 0.003 – 60 µM.
	Confirmation of hit purity and structure	Representative compounds from top structural clusters were re-sourced, characterized for identity and purity by UPLC-MS/UV/ELSD, and evaluated in secondary assays.
	Additional comments	More details are provided in the supplementary information

39

Supplementary Table 2. Crystal structure data collection and refinement statistics

	DCN1:NAcM-HIT 5V83.pdb	DCN1:NAcM-OPT 5V86.pdb	DCN1:NAcM-COV 5V88.pdb	DCN4:CUL1^{WHB} 5V89.pdb
Data collection				
Space group	P21	P21	P21	C2
Cell dimensions				
a, *b*, *c* (Å)	34.966, 97.280, 58.148	35.045, 59.302, 105.83	35.392, 59.181, 104.83	118.93, 38.58, 105.48
α, β, γ (°)	90.0, 104.392, 90.0	96.849, 90, 90	98.677, 90, 90	62.476, 90, 90
Resolution (Å)	50.0-2.00 (2.07-2.00)	50.0-1.37 (1.42- 1.37)	50.0-1.60 (1.66-1.60)	50.0-1.55 (1.61-1.55)
R_{sym} or R_{merge}	7.5 (61.5)	6.9 (44.7)	3.5 (28.3)	7.2 (43.2)
$I / \sigma I$	13.77 (2.24)	15.94 (2.33)	13.37 (2.30)	11.97 (1.48)
Completeness (%)	99.93 (99.33)	97.56 (90.55)	93.57 (80.56)	93.36 (60.65)
Redundancy	3.8 (3.7)	3.2 (2.4)	1.8 (1.7)	3.5 (2.0)
Refinement				
Resolution (Å)	48.74 - 2.0	25.18 - 1.374	28.52 – 1.601	23.92 – 1.550
No. reflections	25,390	77,074	48,264	36,927
R_{work} / R_{free}	0.1715/0.2290	0.1554/0.1950	0.1593/0.1885	0.1503/0.1944
No. atoms				
Protein	2925	2927	2953	2120
Ligand/ion	27	29	37	
Water	293	581	472	312
B-factors				
Protein	38.40	23.30	31.90	25.30
Ligand/ion	47.00	22.20	28.90	
Water	43.60	39.60	43.90	34.60
R.m.s. deviations				
Bond lengths (Å)	0.011	0.013	0.011	0.009
Bond angles (°)	1.27	1.40	1.32	1.13

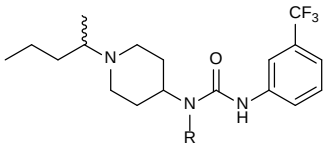

No	R	IC_{50} (μM) (TR-FRET)[1]	% Covalent by MS Analysis	No	R	IC_{50} (μM) (TR-FRET)[1]	% Covalent by MS Analysis
4	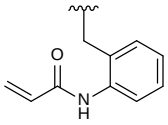	0.041 ± 0.008	100%	**5**	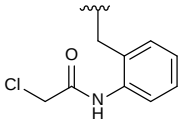	0.256 ± 0.062	10%
6	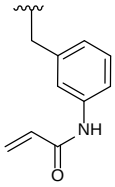	0.098 ± 0.040	0%	**7**	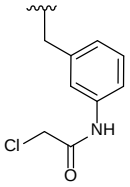	0.076 ± 0.029	10%
8	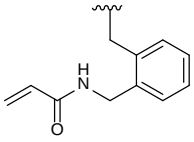	0.135 ± 0.129	10%	**9**	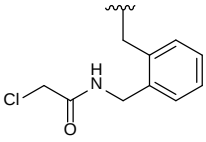	0.222 ± 0.087	0%
10	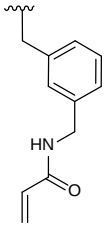	0.066 ± 0.038	0%	**11**	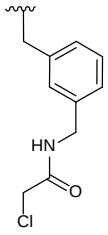	0.028 ± 0.038	0%
12	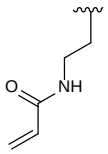	> 34.5	N.D	**13**	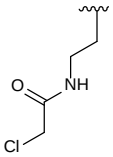	23.6 ± 1.76	N.D
14	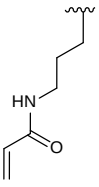	7.50 ± 1.89	N.D	**15**	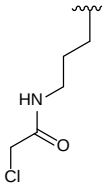	7.74 ± 0.039	N.D

Supplementary Table 3. Optimization of a covalent inhibitor targeting Cys115 of DCN1. Compounds were prepared using slightly modified variants of the synthetic route used to prepare NAcM-COV and NAcM-COVCTRL detailed within the Supplementary Note and purified to > 90% as determined by ELSD/UV prior to testing. [1]The TR-FRET assay used a modified procedure in which samples were incubated for 24 hours prior to measuring the TR-FRET signal to afford sufficient time for covalent linkage to occur.

Potency values for the TR-FRET experiment are represented as means plus or minus standard deviation calculated from one independent experiment, run in triplicate. Compounds that showed significant potency in the TR-FRET assay were selected for further analysis by MaxEnt LC-TOF (time-of-flight) spectra after incubation of DCN1 (30 μM) with DMSO as control or test articles (60 μM) overnight at 4 °C. The results from these MS studies are reported as the qualitative efficiency (% Bound by MS) of test articles to promote formation of a covalent bond with DCN1 as determined by mass shift. ND indicates values were not determined. Compounds were synthesized and tested as racemic mixtures and their characterization can be found in the Supplementary Note.

Supplementary Figure 1

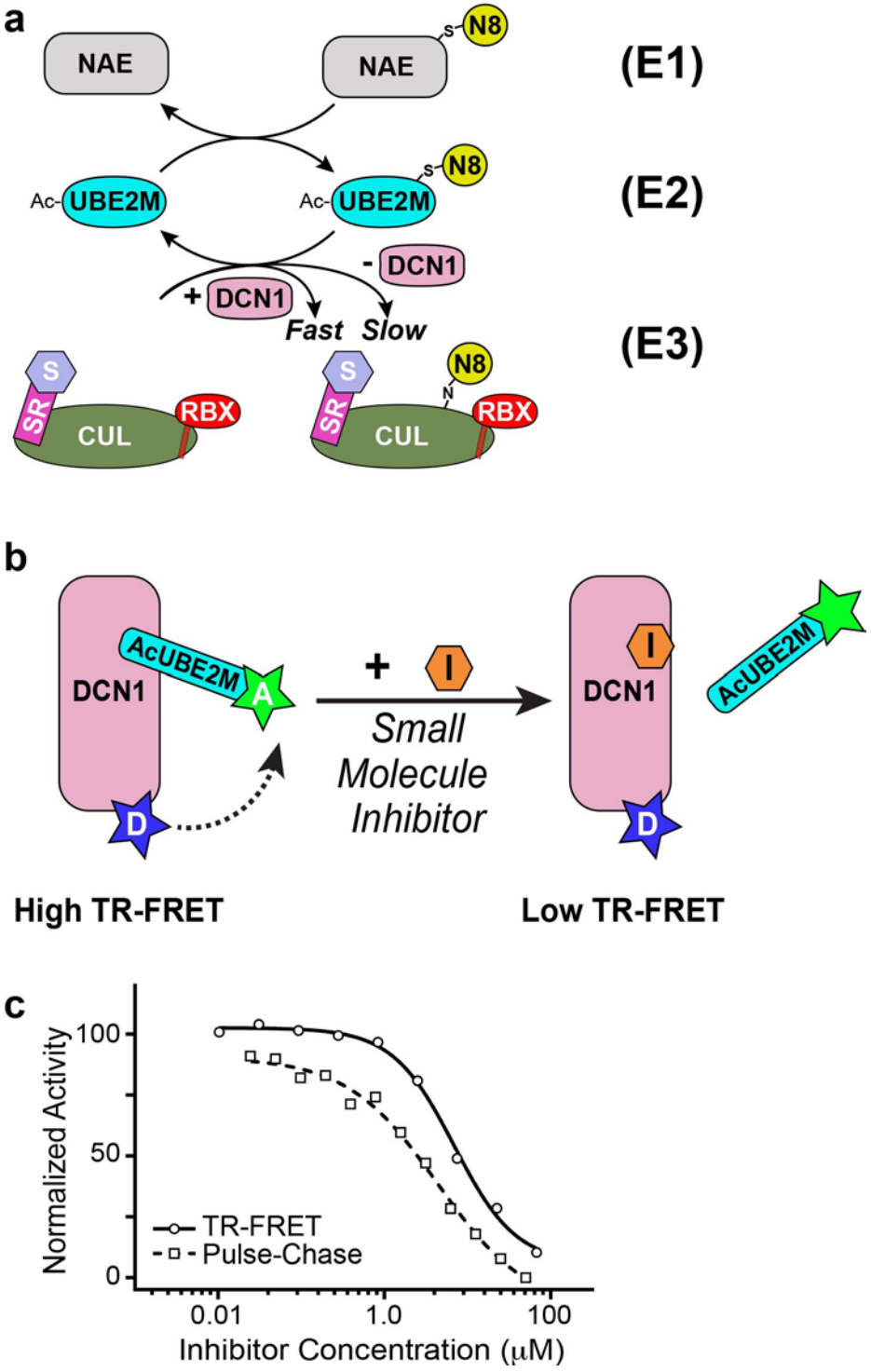

Supplementary Figure 1. Targeting a N-acetyl dependent protein complex in the neddylation enzyme cascade.
(a) Schematic showing role of interaction between N-terminally acetylated UBE2M and DCN1 in the enzymatic cascade leading to cullin Neddylation. NEDD8 is activated and transferred from its E1 to the E2 UBE2M. NEDD8 is subsequently transferred from

UBE2M to a conserved lysine residue in a CUL protein in complex with RBX1, Substrate Receptor (SR), and Substrate (S). The reaction is accelerated by DCN1 binding to UBE2M's acetylated N-terminus.
(b) Schematic of TR-FRET assay used for HTS. High TR-FRET signal is observed between Tb-DCN1 and Alexa-fluor488-labeled AcUBE2M. A competing inhibitor results in dissociation of AcUBE2M and Low TR-FRET signal.
(c) Dose-response assays monitoring NAcM-HIT activity in TR-FRET (o - IC_{50} = 6.91 ± 0.442 μM) or pulse-chase assay (□- IC_{50} = 4.36 ± 0.150 μM). These are representative examples from multiple biological replicates. Each graphed example represents a single biological replicate carried out in technical triplicate.

Supplementary Figure 2

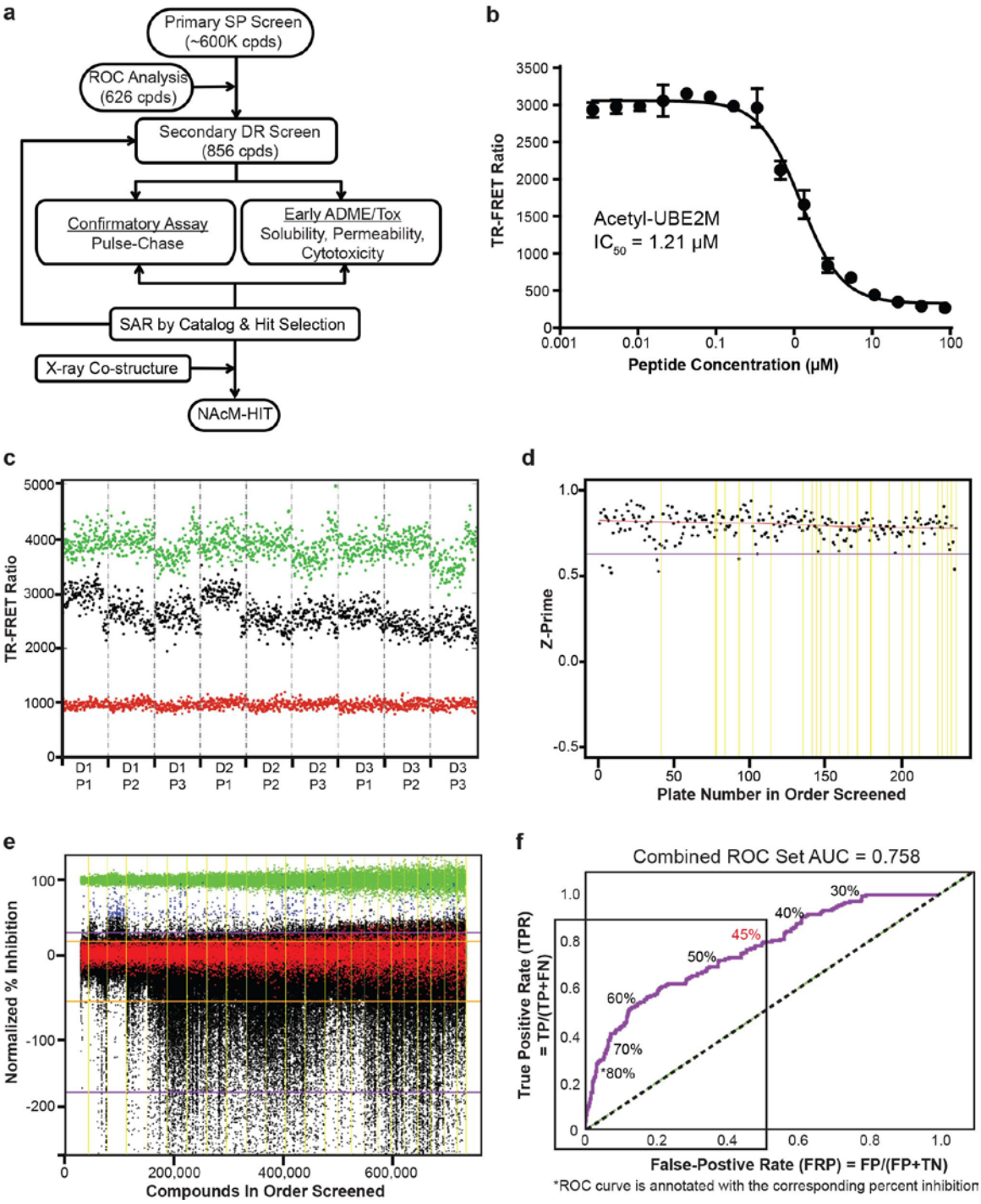

Supplementary Figure 2. Summary and quality control data for the high-throughput screening campaign to identify a lead compound antagonizing N-terminal acetyl UBE2M binding to DCN1.

(a) Schematic of HTS workflow

(b) Validation of our high-throughput ligand competition assay measuring the TR-FRET signal between a biotinylated version of DCN1, recognized by terbium-linked streptavidin, and a stapled peptide corresponding to N-terminally acetylated UBE2M labeled at its C-terminus with AlexaFluor 488 by competition with an unlabeled variant of the acetylated UBE2M peptide. Potency value represents the mean from one independent experiment, run in triplicate.
(c) Signal profiles (high-green, medium-black, and low-red) acquired during the assay validation, demonstrating the reproducibility of the assay over multiple days (D1 P1 abbreviation corresponds to Day 1, Plate 1).
(d) Z-prime values calculated for each plate of the screen using plate level internal controls.
(e) Scatter plot of primary screen data shown as normalized percent inhibition. Each dot represents the activity of one compound and controls represent plate matched in plate controls (positive control, unlabeled UBE2M peptide (green); negative control, DMSO (red), and test compounds (hits blue and non-hits black) under the TR-FRET assay.
(f) Receiver operating characteristic (ROC) curve. The X-axis shows the false positive rate and the left Y-axis shows the true positive rate. A true positive was defined as a compound that produced a well-behaved sigmoidal inhibitory curve from a dose-response experiment using the primary assay. The curve is annotated with the corresponding percent inhibition. The assay has good discriminatory power (area under the curve = 0.74 with 95% confidence interval between 0.72 and 0.76). For reference, a perfect assay would have AUC 1.0, whereas a random assay has AUC of 0.5. Hit criteria of > 45% captures roughly 80% of the true positives based on the ROC analysis and was chosen empirically as the hit cutoff. A significant number of true hits likely remain in the band from beyond the 45% cut-off activity, and these compounds were not considered in this manuscript.

Supplementary Figure 3

a

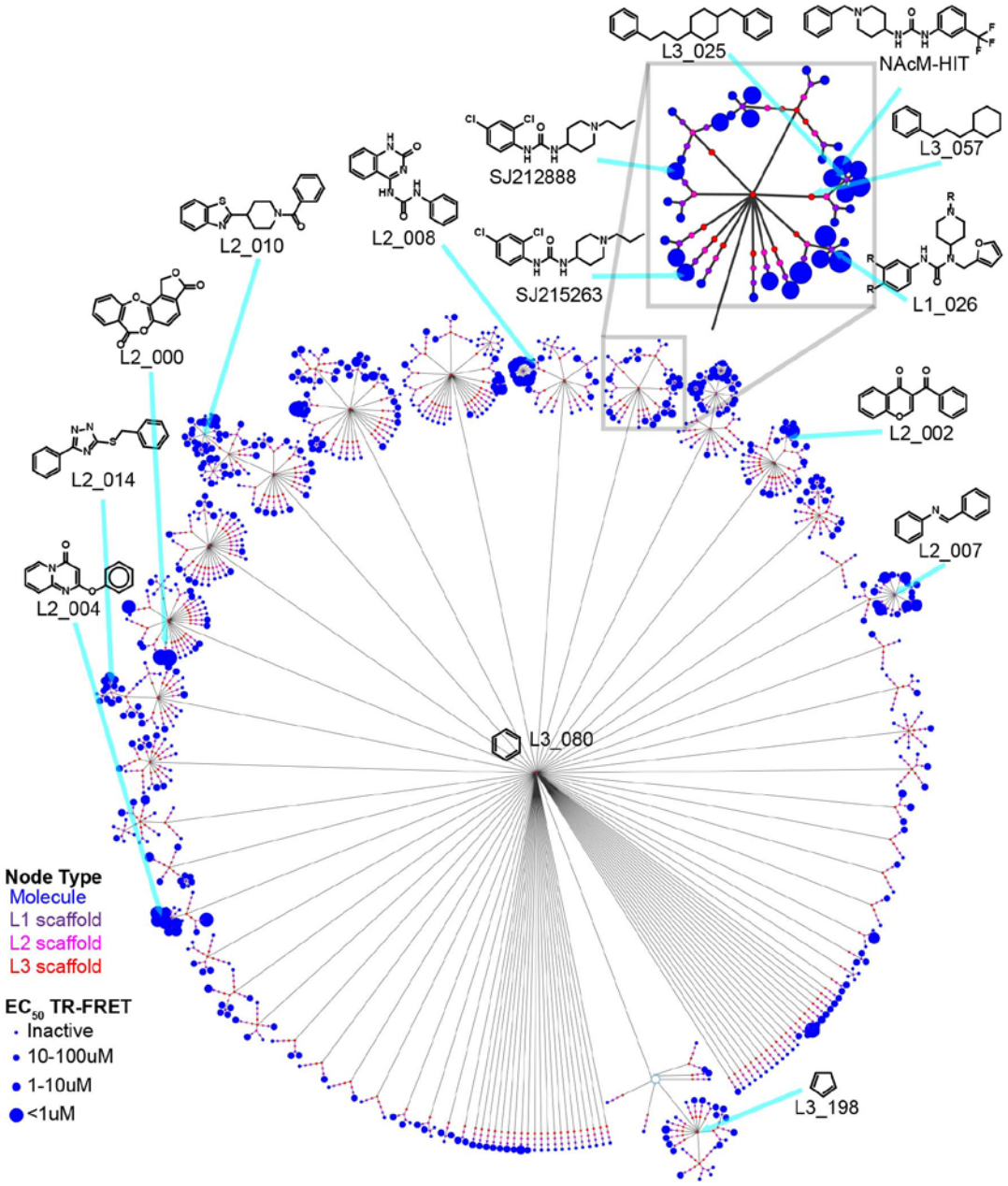

b

SJ212329 (NAcM-HIT)	SJ342767	SJ431244
IC_{50} = 6.91 ± 0.441 µM (TR-FRET)	IC_{50} = 13.5 ± 5.28 µM (TR-FRET)	IC_{50} = 8.71 ± 0.655 µM (TR-FRET)
EC_{50} = 4.2 µM (Pulse-Chase)	EC_{50} = 2.8 µM (Pulse-Chase)	EC_{50} = 0.572 µM (Pulse-Chase)
Cytotox. = > 24.1 µM (BJ Cells)	Cytotox. = > 15.3 µM (BJ Cells)	Cytotox. = > 16.8 µM (BJ Cells)
Sol. = 31.8 ± 1.6 µM	Sol. = 11.4 ± 0.4 µM	Sol. = 0.3 ± 0.3 µM
Perm. = 1280 ± 270 x10^{-6} cm/s	Perm. = 911 ± 145 x10^{-6} cm/s	Perm. = 1170 ± 323 x10^{-6} cm/s

139

Supplementary Figure 3. Identification and validation of a top scaffold from the high-throughput screening (HTS) campaign.
(a) Network graph showing the chemical structure clusters from some of the 182 validated hits. Topologically similar molecules cluster together in the branches of the network. To construct the graph, molecules were first abstracted to scaffolds and then further to cores using the Murcko algorithm. Each of these structural entities is represented as a node, and nodes are connected via edges according to topological relationships with closeness being defined using the Tanimoto coefficient. Molecular nodes are coded to reflect potency based on size. The top half of the figure provides greater detail on some of the potent chemotypes and highlights the well-developed structure activity relationships that existed for the scaffold represented by NAcM-HIT. (b) Representative members of the top three hit clusters identified from our HTS campaign. The shared N-benzyl (or benzoyl) piperidine pharmacophore element is highlighted in red. These scaffolds were chosen based on the combination of reasonable potency (IC_{50} < 10 µM), evident SAR from analogs embedded in the screening set, and the perception that they might lend themselves to optimization. Values for the TR-FRET, solubility, permeability, and cytotoxicity experiments are represented as means plus or minus standard deviation calculated from one independent experiment, run in triplicate. Pulse-chase data were generated from a single experiment. There were more than 300 compounds containing this pharmacophore element included within our screening collection (Supplementary Dataset 2).

Supplementary Figure 4

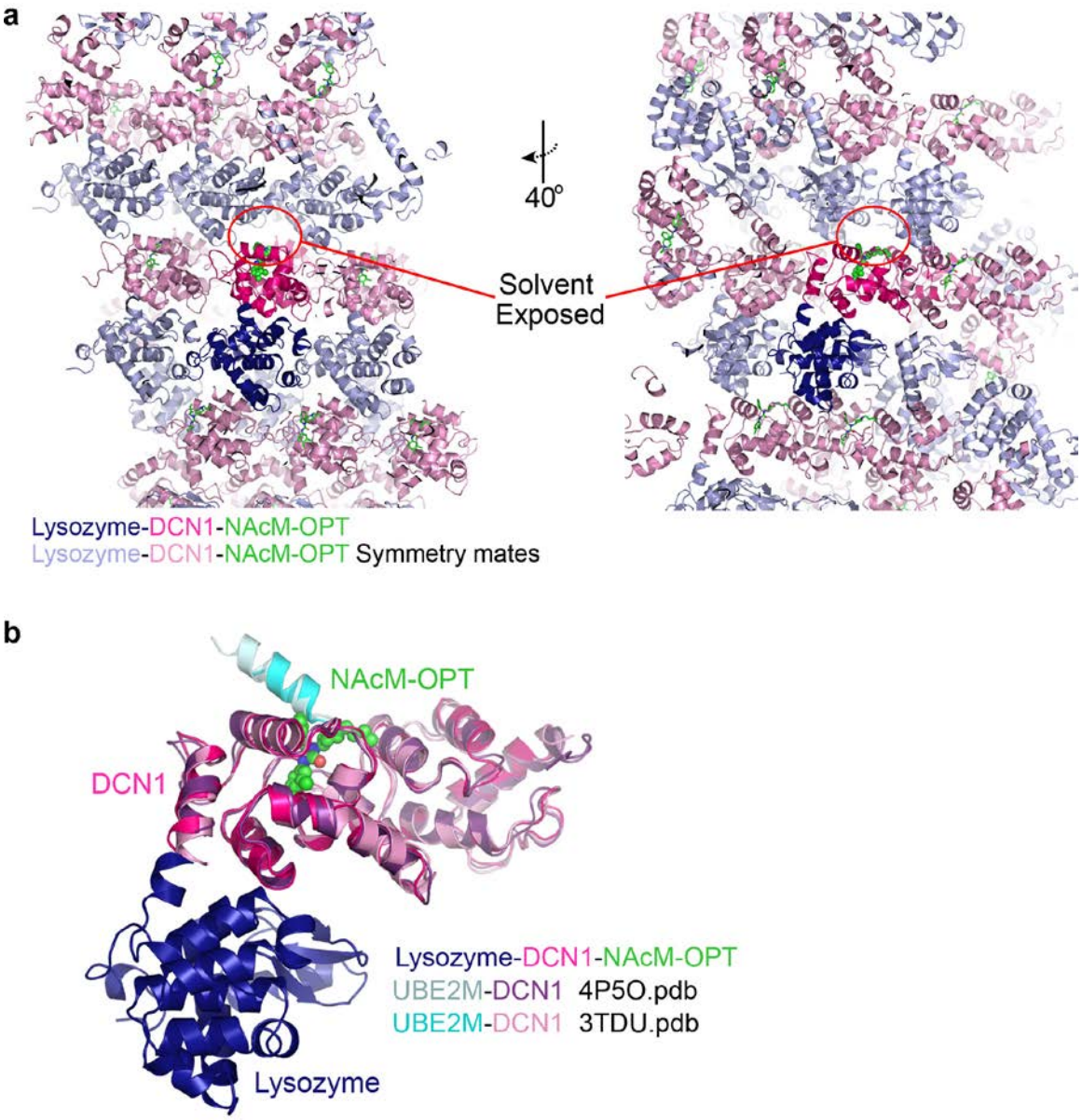

Supplementary Figure 4. Crystal packing and integrity of DCN1 structure in the Lysozyme-DCN1 fusion used for crystallography.
(a) Two views of the crystal lattice in the Lysozyme-DCN1-NAcM-OPT structure demonstrate that the DCN1-NAcM-OPT binding pocket is solvent exposed and free of crystal packing artifacts. A single copy of Lysozyme (blue)-DCN1 (hot pink)-NAcM-OPT (green) in the asymmetric unit is shown and symmetry mates within the lattice colored light blue, pink, and green respectively.
B. Fusion of Lysozome to the amino terminus of DCN1 does not alter the overall fold of DCN1. Structural superposition of DCN1 from the Lysozyme (blue)-DCN1 (hot pink)-NAcM-OPT (green) structure with full-length DCN1 (purple)-AcUBE2M (pale cyan, 4P5O.pdb) and the AcUBE2M peptide bound to DCN1 (pink)-AcUBE2M (cyan, 3TDU.pdb).

Supplementary Figure 5

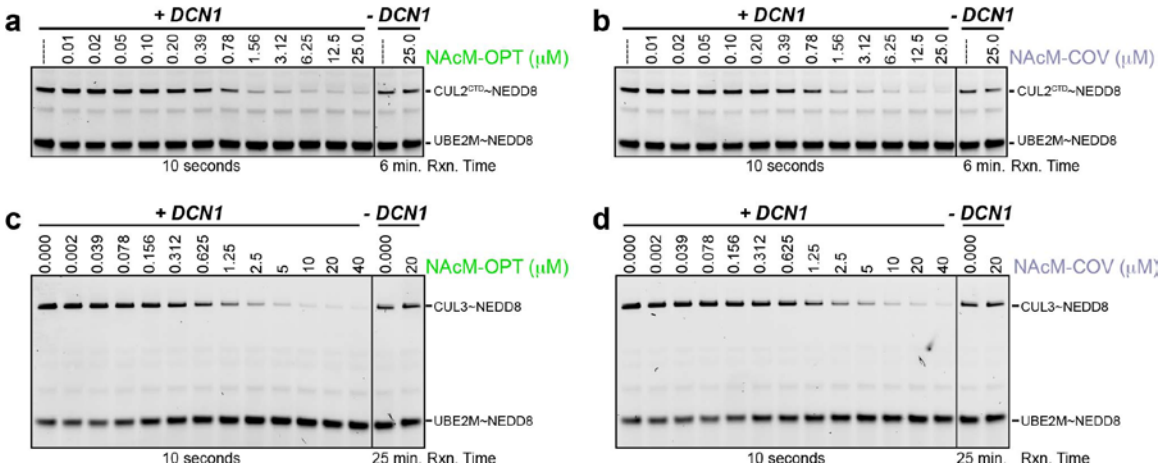

Supplementary Figure 5. Dose response pulse-chase assays for NAcM-OPT and NAcM-COV inhibition of DCN1 dependent neddylation of CUL2^{CTD}-RBX1 and CUL3-RBX1.

(a) Fluorescent scan of gels from pulse-chase assay monitoring the dose response inhibition of CUL2^{CTD}-RBX1 neddylation by the indicated concentrations of NAcM-OPT after pre-incubation with DCN1 for 30 minutes at 4 °C.

(b) Same as (a), but with NAcM-COV.

(c) Same as (a), but monitoring neddylation of full-length CUL3-RBX1.

(d) Same as (c), but with the NAcM-COV.

Supplementary Figure 6

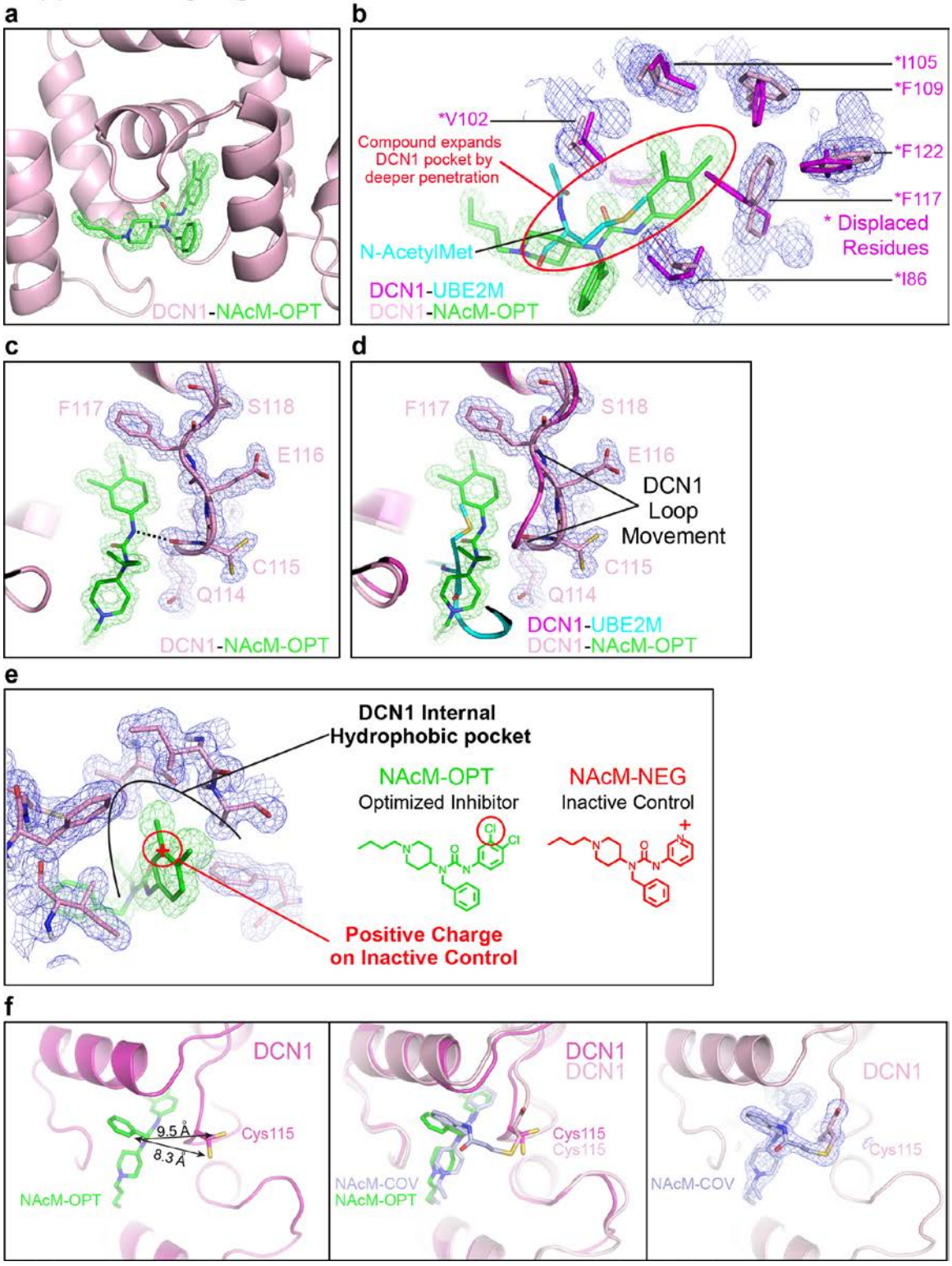

Supplementary Figure 6. Structural features and rearrangements of the N-Acetyl-Met binding pocket in NAcM bound DCN1.

(a) Simulated annealing omit map of Fo-Fc density (green mesh, 3.0σ) surrounding NAcM-OPT (green, sticks) in the DCN1-NAcM-OPT structure.
(b) Displacement of internal amino acids lining the N-Acetyl-Met binding pocket of DCN1 upon NAcM-OPT binding. Shown is simulated annealing omit map (Fo-Fc, green mesh, 3.0σ; 2Fo-Fc, blue mesh, 1.0α) around the DCN1 (pink sticks)-NAcM-OPT (green, sticks) structure superimposed to DCN1 (purple, sticks)-AcUBE2M (cyan, sticks) from 3TDU.pdb. Internal binding pocket residues that are displaced are highlighted. The red oval highlights generation of a deeper N-Acetyl-Met binding pocket upon inhibitor binding relative to previous DCN1 structures.
(c) Backbone residues from DCN1's Gln114 form a critical hydrogen bond with the urea aryl N-H from bound inhibitor. Shown is the simulated annealing omit map (Fo-Fc, green mesh, 3.0σ: 2Fo-Fc, blue mesh, 1.0α) around the DCN1 (pink, sticks)- NAcM-OPT(green, sticks). The dashed line demarks the hydrogen bond interaction formed between DCN1's Gln114 backbone and the urea aryl N-H of NAcM-OPT.
(d) Same as (c), but structural superposition to DCN1 (purple cartoon)-AcUBE2M (cyan sticks) from 3TDU.pdb highlighting conformational rearrangements within a flexible loop (residues 114-117) of DCN1 upon NAcM-OPT binding.
(e) Rationale for the design of an inactive control analog. Shown is the simulated annealing omit map (Fo-Fc, green mesh, 3.0σ: 2Fo-Fc, blue mesh, 1.0α) around the DCN1 (pink, sticks)-NAcM-OPT (green, sticks) structure. DCN1's hydrophobic pocket surrounding the inhibitor and corresponding position of the ionizable pyridine ring of the inactive control NAcM-NEG are highlighted.
(f) Structure based covalent targeting of DCN1's Cys115 for development of a covalent inhibitor. Left panel - Structure of DCN1 (hot pink)-NAcM-OPT (green, sticks) with Cys115 of DCN1 in sticks. Distances between the ortho-N-acrylamide substitution and Cys115 are shown. Middle panel - Superposition of DCN1 (hot pink)-NAcM-OPT (green, sticks) and DCN1 (pink)-NAcM-COV (light blue sticks) with the covalent linkage to Cys115 shown in sticks. Right panel - 2Fo-Fc density surrounding NAcM-COV (light blue, sticks) and Cys115 (pink sticks) in the DCN1-NAcM-COV structure.

Supplementary Figure 7

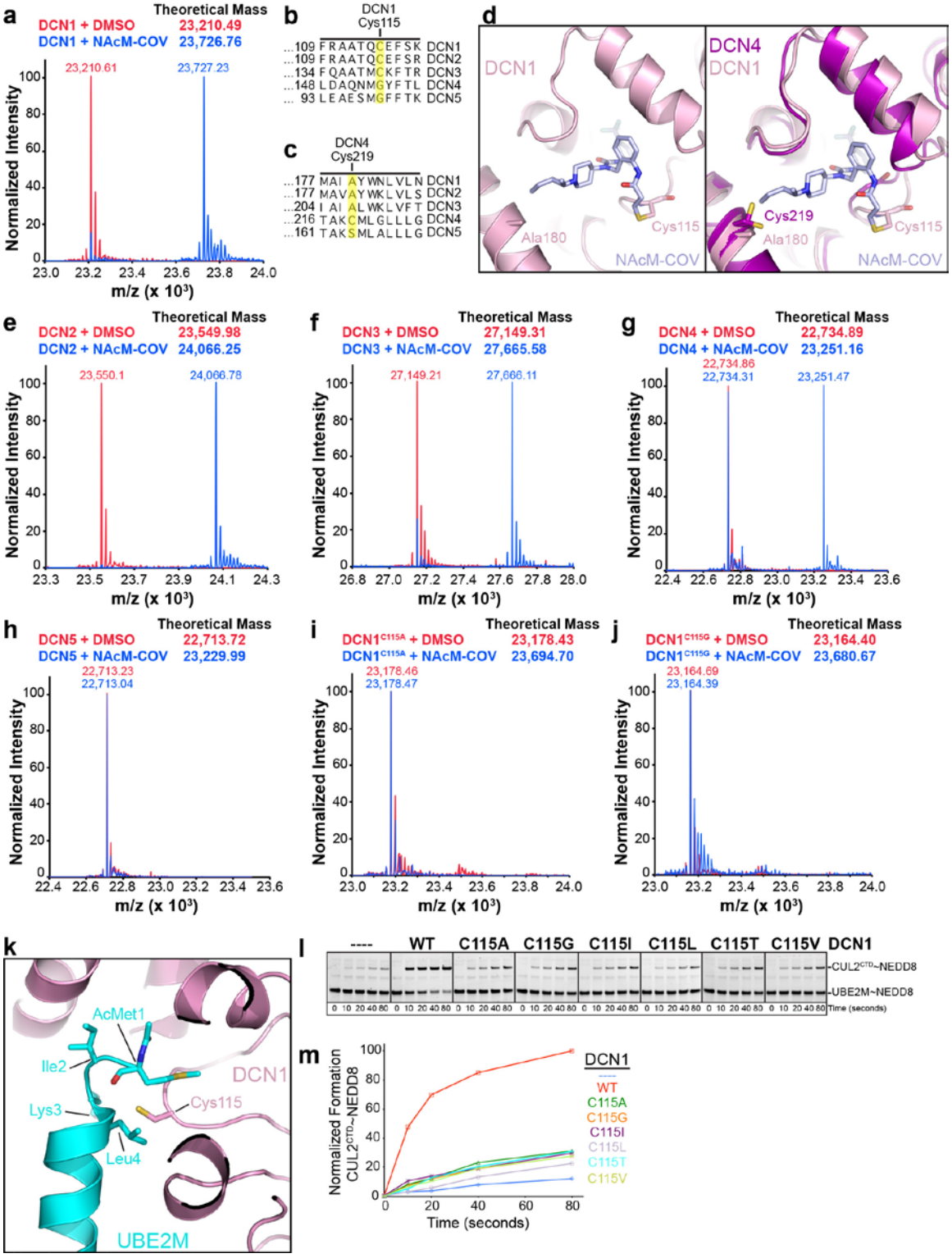

Supplementary Figure 7. Covalent adduct formation, DCN1 residue targeting, and DCN family selectivity of the covalent inhibitor NAcM-COV.

(a) MaxEnt LC-TOF (time-of-flight) spectra after incubation of DCN1 (30 μM) with DMSO (red spectrum) or NAcM-COV (60 μM) (blue spectrum) overnight at 4 °C. Incubation with NAcM-COV shifts the mass of DCN1 ~+516.27 da, consistent with formation of a DCN1-NAcM-COV covalent adduct.
(b) Structure based sequence alignment of the DCN family members surrounding the NAcM-COV targeted Cys115 of DCN1.
(c) Structure based sequence alignment of the DCN family members surrounding the presumed NAcM-COV targeted Cys219 of DCN4.
(d) Cysteine targeting of DCN4 by NAcM-COV. Left panel – Structure of DCN1 (pink)-NAcM-COV (light blue, sticks) with the covalent linkage between NAcM-COV and DCN1's Cys115 and the position of Ala180 highlighted. Right panel – same as left panel, but with alignment of DCN4. The potential targeted Cys of DCN4 (Cys219) is highlighted.
(e) Same as (a), but with DCN2.
(f) Same as (a), but with DCN3.
(g) Same as (a), but with DCN4.
(h) Same as (a), but with DCN5.
(i) Same as (a), but with C115A DCN1.
(j) Same as (a), but with C115G DCN1.
(k) Cys115 of DCN1 is part of a critical interaction surface with AcUBE2M. Structure of DCN1(pink)-AcUBE2M (cyan, sticks) from 3TDU.pdb highlighting the position of Cys115 from DCN1 nestled between N-AcMet1 and Leu4 of UBE2M.
(l) Fluorescent scan of gels from pulse-chase assay monitoring the stimulation of $Cul2^{CTD}$-RBX1 neddylation by WT and the indicated Cys115 mutants of DCN1.
(m) Quantification of the results from (l).

Supplementary Figure 8

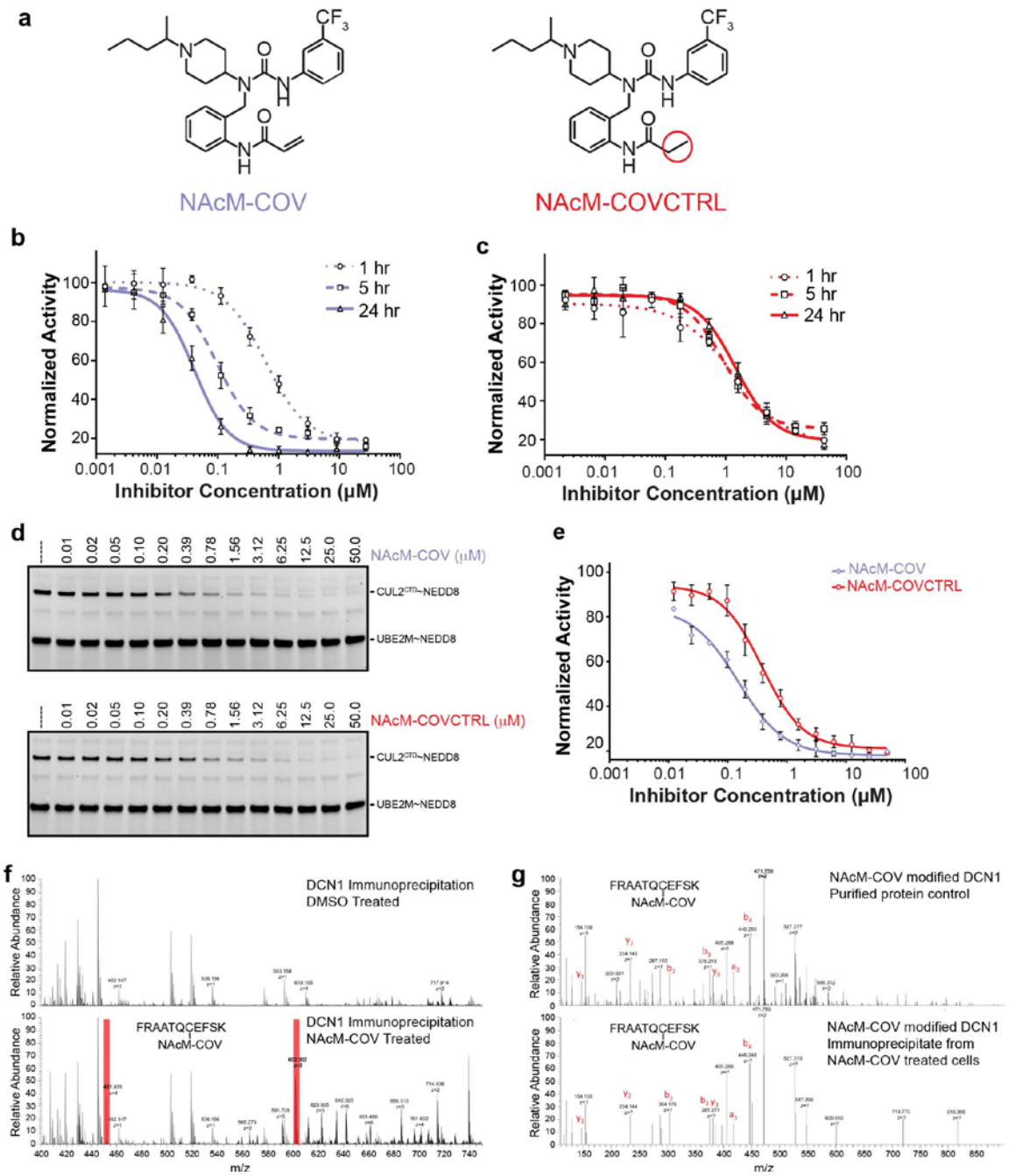

Supplementary Figure 8. Potency of NAcM-COV is dependent on the presence of an electrophilic warhead.

(a) Chemical structures of NAcM-COV and NAcM-COVCTRL, highlighting that in NAcM-COVCTRL the acrylamide warhead is replaced with a propionamide that is incapable of forming a covalent linkage.

(b) Time-course evaluation of the TR-FRET potency for NAcM-COV, demonstrating that potency is increased in a time-dependent manner. NAcM-COV exhibited TR-FRET IC_{50} values of 0.619 ± 0.117 μM after one hour of pre-incubation with DCN1, 0.0969 ± 0.022

μM after five hours of pre-incubation with DCN1, and 0.0413 ± 0.008 μM after 24 hours of pre-incubation with DCN1. These results support the irreversible nature of NAcM-COV binding. Times correspond to different lengths of incubation of the complete TR-FRET assay mixture prior to measuring the TR-FRET signal. Potency values are represented as means plus or minus standard deviation calculated from one independent experiment, run in triplicate.

(c) Time-course evaluation of the TR-FRET potency for NAcM-COVCTRL, demonstrating that potency is not increased in a time-dependent manner. NAcM-COVCTRL exhibited TR-FRET IC_{50} values of 1.34 ± 0.152 μM after one hour of pre-incubation with DCN1, 0.931 ± 0.049 μM after five hours of pre-incubation with DCN1, and 1.46 ± 0.237 μM after 24 hours of pre-incubation with DCN1. Times correspond to different lengths of incubation of the complete TR-FRET assay mixture prior to measuring the TR-FRET signal. Potency values are represented as means plus or minus standard deviation calculated from one independent experiment, run in triplicate.

(d) Fluorescent scan of gels from pulse-chase assay monitoring the dose response inhibition of $CUL2^{CTD}$-RBX1 neddylation by the indicated concentrations of NAcM-OPT or NAcM-COVCTRL after pre-incubation with DCN1 overnight at 4 °C.

(e) Quantification of the results from panel d. NAcM-COV exhibited a pulse-chase IC_{50} value of 0.151 ± 0.011 μM and NAcM-COVCTRL exhibited a pulse-chase IC_{50} value of 0.382 ± 0.051 μM after 24 hours of pre-incubation with DCN1. Plotted are the averages of three independent experiments.

(f) MS1 spectra averaged over the course of the elution profile of the NAcM-COV modified FRAATQCEFSK from DCN1 immunoprecipitates from cell treated with DMSO (top panel) or NAcM-COV (bottom panel). Highlighted in red are the triply and quadruply charged precursors of NAcM-COV modified FRAATQCEFSK.

(g) Product ion spectra after HCD activation of the quadruply charged precursor (m/z 451.73) from NAcM-COV treated DCN1 purified protein (top panel) or DCN1 immunoprecipitates from NAcM-COV treated cells (bottom panel).

Supplementary Figure 9

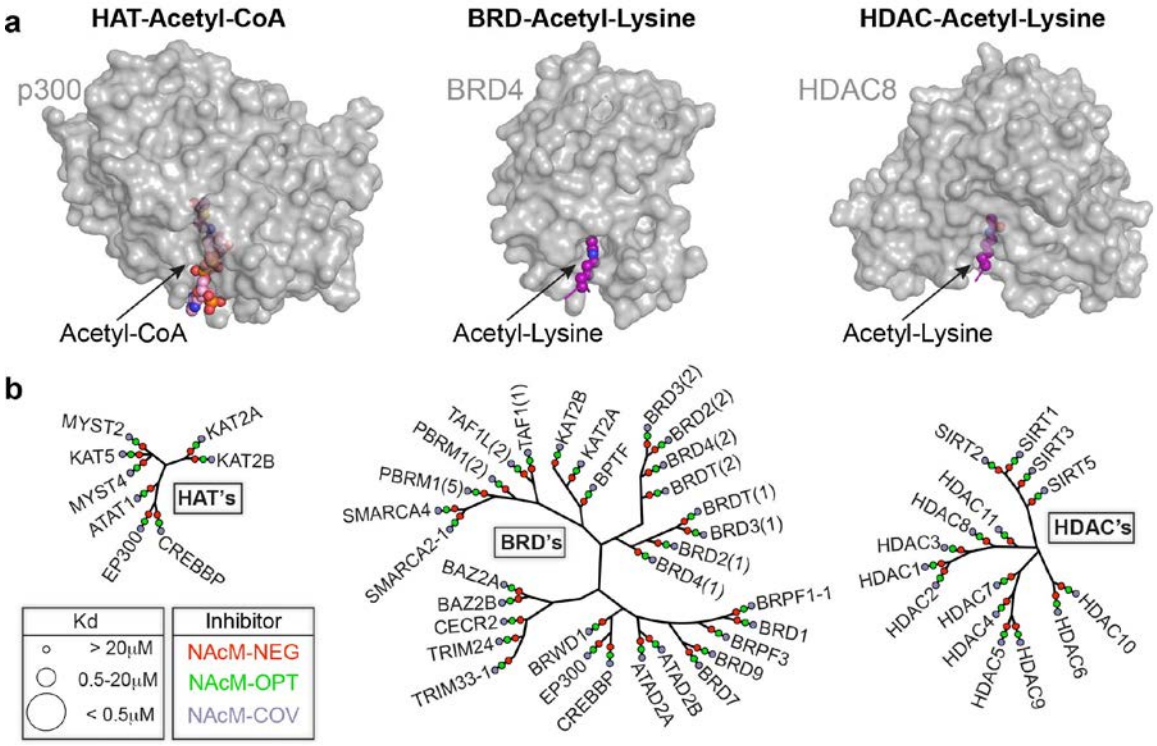

Supplementary Figure 9. NAcM inhibitors do not inhibit the activity of Histone Acetyltransferases, Bromodomains, or Histone Deacetylases.

(a) Structural views of other Acetyl dependent protein interactions. Left panel – Histone acetyl transferases (HATs) as represented by p300 (gray, surface)- Acetyl-CoA (purple, spheres) from 4PZS.pdb. Center panel – Bromodomains (BRDs) as represented by BRD4(1) (gray, surface)- Histone H4 K5Ac (purple, spheres) from 3UVW.pdb. Right panel – Histone deacetylases (HDACs) as represented by HDAC8 (gray, surface)- K8Ac (purple, spheres) from 2V5W.pdb.

(b) NAcM-NEG (red), NAcM-OPT (green), and NAcM-COV (light blue) were tested at a single concentration of 10 μM against a panel of HAT's (left panel), BRD's (center panel) and HDAC's (right panel). Any interaction apparently inhibited by > 40% in the screening test was subjected to duplicate dose-response studies using the same assays. No interaction was significantly inhibited by any test compound. Inferred binding Kd's for each inhibitor tested, as determined from percent of control inhibition values, are plotted on similarity based dendrogram diagrams for each family member tested (Supplemental Dataset 3-5).

Supplementary Figure 10

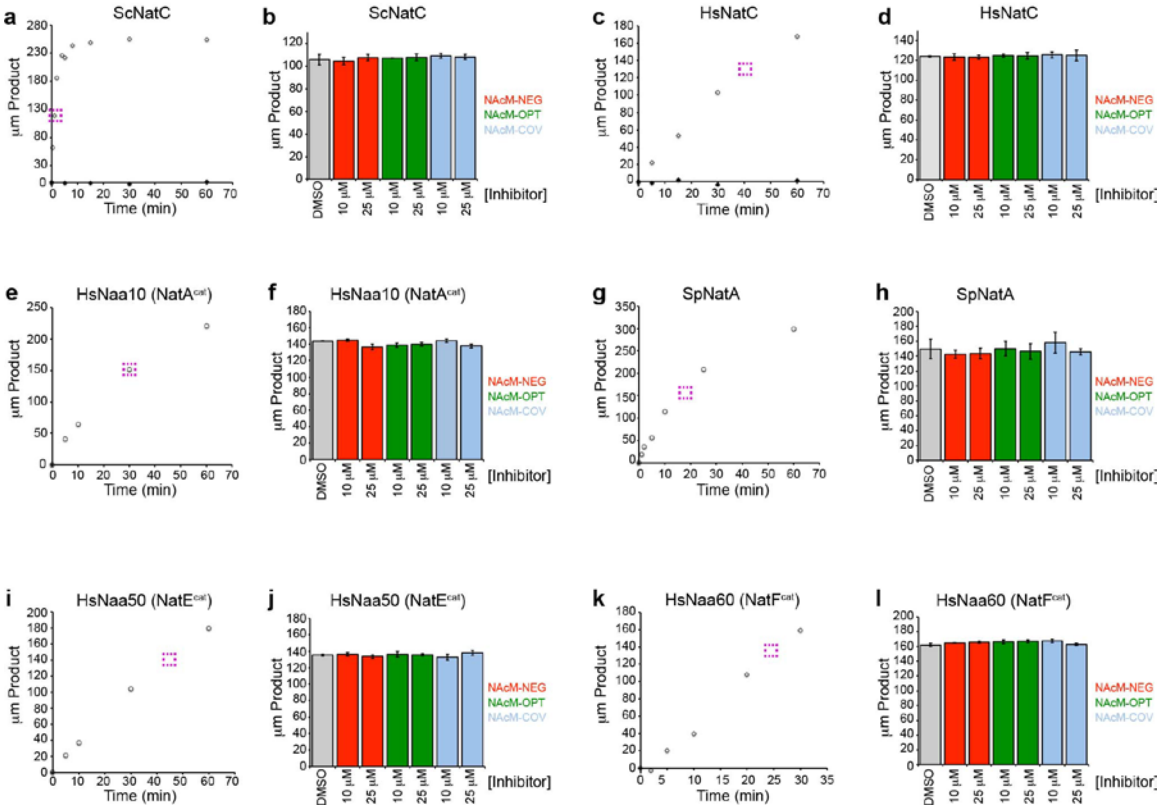

Supplementary Figure 10. NAcM inhibitors do not inhibit the activity of N-terminal acetyltransferases.

(a) Time-course assay following product formation over time for N-terminal acetylation of the peptide substrate NH_2-MIKLFSLKQQKKEEESAGGTKGSSKK by the yeast NatC complex. The dashed purple square marks the time point chosen for subsequent assays to evaluate the effect of NAcM inhibitors.
(b) Product formation by the yeast NatC complex in the absence or presence of the indicated concentrations of NAcM inhibitors. The results are from one independent experiment repeated in triplicate.
(c) Same as (a), but with the human NatC complex.
(d) Same as (b), but with the human NatC complex.
(e) Time-course assay following product formation over time for N-terminal acetylation of the peptide substrate NH_2-EEEIAALRWGRPVGRRRRPVRVYP by hNaa10, the catalytic subunit of the human NatA complex. The dashed purple square marks the time point chosen for subsequent assays to evaluate the effect of NAcM inhibitors.
(f) Product formation by hNaa10 in the absence or presence of the indicated concentrations of NAcM inhibitors. The results are from one independent experiment repeated in triplicate.
(g) Time-course assay following product formation over time for N-terminal acetylation of the peptide substrate NH_2-SESSSKSRWGRPVGRRRRPVRVYP by the NatA complex from *Schizosaccharomyces pombe*. The dashed purple square marks the time point chosen for subsequent assays to evaluate the effect of NAcM inhibitors.
(h) Product formation by *Schizosaccharomyces pombe* NatA complex in the absence or presence of the indicated concentrations of NAcM inhibitors. The results are from one independent experiment repeated in triplicate.

(i) Time-course assay following product formation over time for N-terminal acetylation of the peptide substrate NH_2-MLGPEGGRWGRPVGRRRRPVRVYP by hNaa50, the catalytic subunit of the human NatE complex. The dashed purple square marks the time point chosen for subsequent assays to evaluate the effect of NAcM inhibitors.
(j) Product formation by hNaa50 in the absence or presence of the indicated concentrations of NAcM inhibitors. The results are from one independent experiment repeated in triplicate.
(k) Time-course assay following product formation over time for N-terminal acetylation of the peptide substrate NH_2-MAPLDLDRWGRPVGRRRRPVRVYP by hNaa60, the catalytic subunit of the human NatF complex. The dashed purple square marks the time point chosen for subsequent assays to evaluate the effect of NAcM inhibitors.
(l) Product formation by hNaa60 in the absence or presence of the indicated concentrations of NAcM inhibitors. The results are from one independent experiment repeated in triplicate.

Supplementary Figure 11

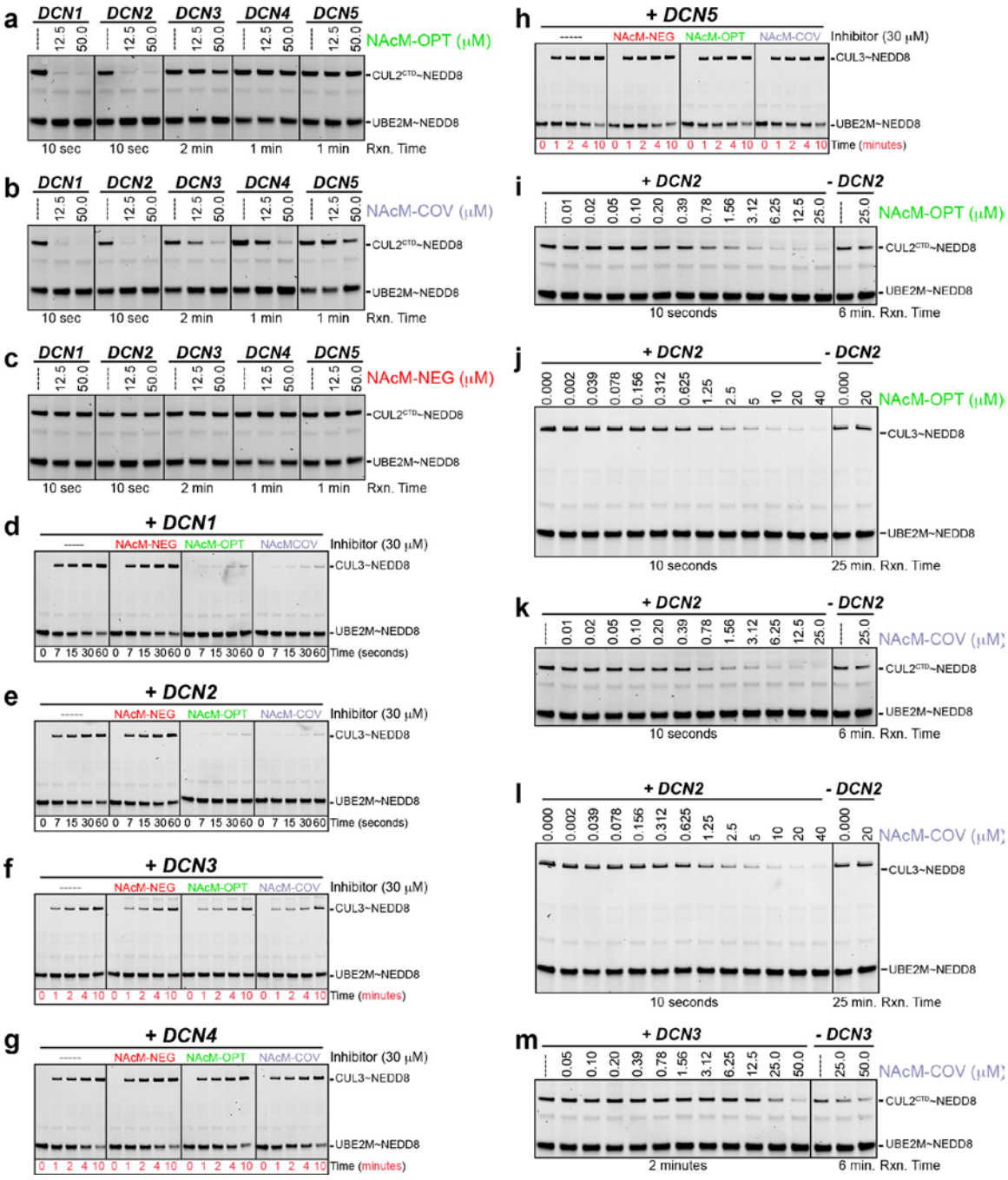

Supplementary Figure 11. Isoform selectivity of NAcM inhibitors towards DCN family members.

(a) Fluorescent scan of gels from pulse-chase assay monitoring the effects of the indicated concentrations of NAcM-OPT on the indicated DCN family member mediated stimulation of $Cul2^{CTD}$-RBX1 neddylation.

(b) Same as (a), but with NAcM-COV.

(c) Same as (a), but with NAcM-NEG.

(d) Fluorescent scan of gels from pulse-chase assay monitoring the effects of NAcM-NEG, NAcM-OPT, and NAcM-COV at 30 μM on DCN1 dependent neddylation of full-length CUL3-RBX1.
(e) Same as (d), but with DCN2.
(f) Same as (d), but with DCN3.
(g) Same as (d), but with DCN4.
(h) Same as (d), but with DCN5.
(i) Fluorescent scan of gels from pulse-chase assay monitoring the dose-response inhibition of DCN2 mediated stimulation of $Cul2^{CTD}$-RBX1 neddylation by NAcM-OPT.
(j) Same as (I), but with full-length CUL3-RBX1.
(k) Same as (I), but with the NAcM-COV.
(l) Same as (k), but with full-length CUL3-RBX1.
(m) Same as (k), but with DCN3.

Supplementary Figure 12

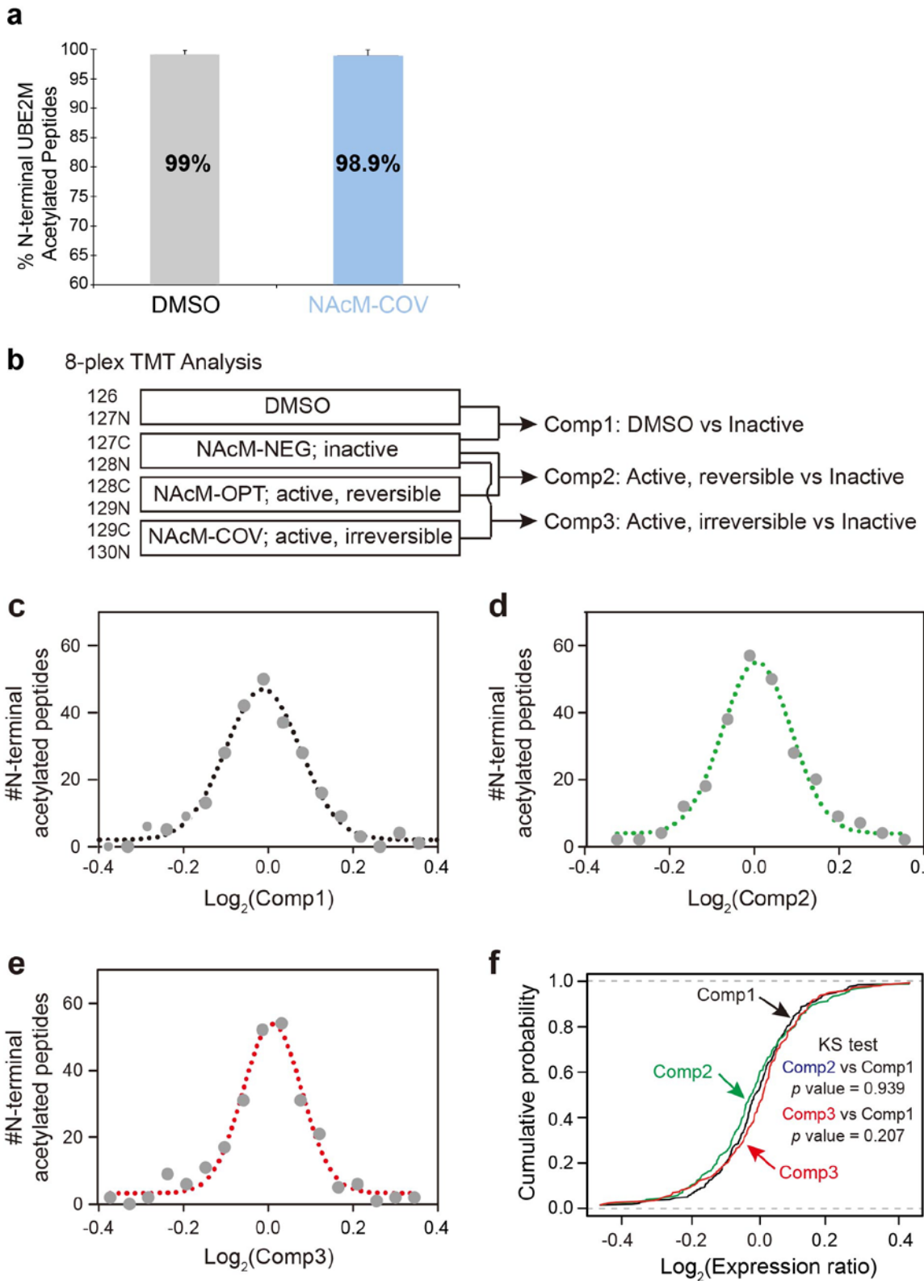

Supplementary Figure 12. NAcM's do not effect N-terminal acetylation in cells.

(a) IP-MS of UBE2M from NAcM-COV treated cells confirming that inhibitor treatment does not alter the acetylation status of UBE2M. 293T cells expressing UBE2M-FLAG-HA were treated for 24 hours with DMSO or 10 μM NAcM-COV. Lysates were subjected to Anti-Flag immunoprecipitation and the extent of UBE2M N-terminal acetylation was determined by mass spec. Results are displayed as the percentage of amino-terminal UBE2M peptides that are acetylated

(b) 8-plex TMT proteomics assay was used to examine effects of the chemicals on N-terminal acetylation. Four conditions were used in this assay, including reversible inhibitor (NAcM-OPT), covalent inhibitor (NAcM-COV), inactive compounds (NAcM-NEG), and DMSO control. Each treatment had two biological replicates.

(c) Distribution of the Log2 expression difference in N-terminal acetylated peptides between NAcM-NEG and DMSO (Comp1). The distribution was fitted with a Gaussian distribution (dotted line).

(d) Distribution of the Log2 expression difference in N-terminal acetylated peptides between NAcM-OPT and NAcM-NEG (Comp2). The distribution was fitted with a Gaussian distribution (dotted line).

(e) Distribution of the Log2 expression difference in N-terminal acetylated peptides between NAcM-COV and NAcM-NEG (Comp3). The distribution was fitted with a Gaussian distribution (dotted line).

(f) Kolmogorov–Smirnov (KS) test shows that there is no statistical difference between Comp2 and Comp1 (p value = 0.939), and between Comp3 and Comp1 (p value = 0.207), as these p values are much higher than a common p value cutoff of 0.05 (95% confidence interval). The KS test was performed using the R statistical package (version 3.3).

Supplementary Figure 13

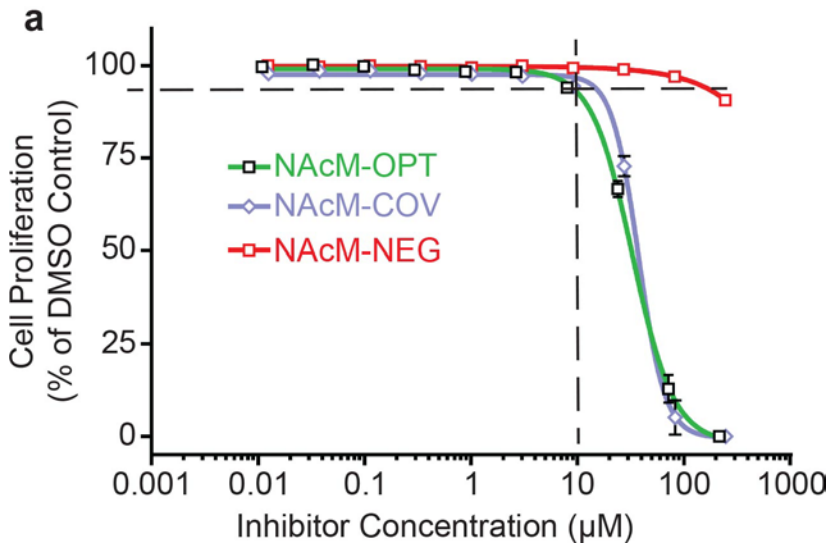

Supplementary Figure 13. NAcM's do not effect proliferation at 10 μM.
(a) Dose-response of inhibitors using CellTiter-Glo cell viability assay for HCC95 cells and demonstrating that NAcM-OPT (LD_{50} 31.8 μM ± 0.350), NAcM-COV (LD_{50} 36.4 μM ± 3.34), and NAcM-NEG (LD_{50} >200 μM), are not overtly toxic or growth inhibitory at the concentration of 10 μM used for other cellular assays (highlighted by dashed lines). Potency values are represented as means plus or minus standard deviation calculated from one independent experiment, run in triplicate.

Supplementary Figure 14

a

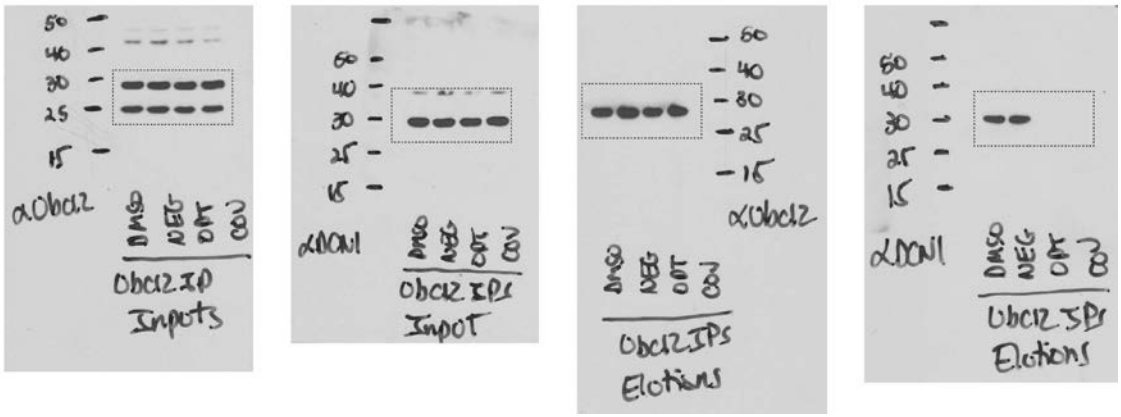

Supplementary Figure 14. Full Gel images for **a.** Figure 4a

Supplementary Figure 15

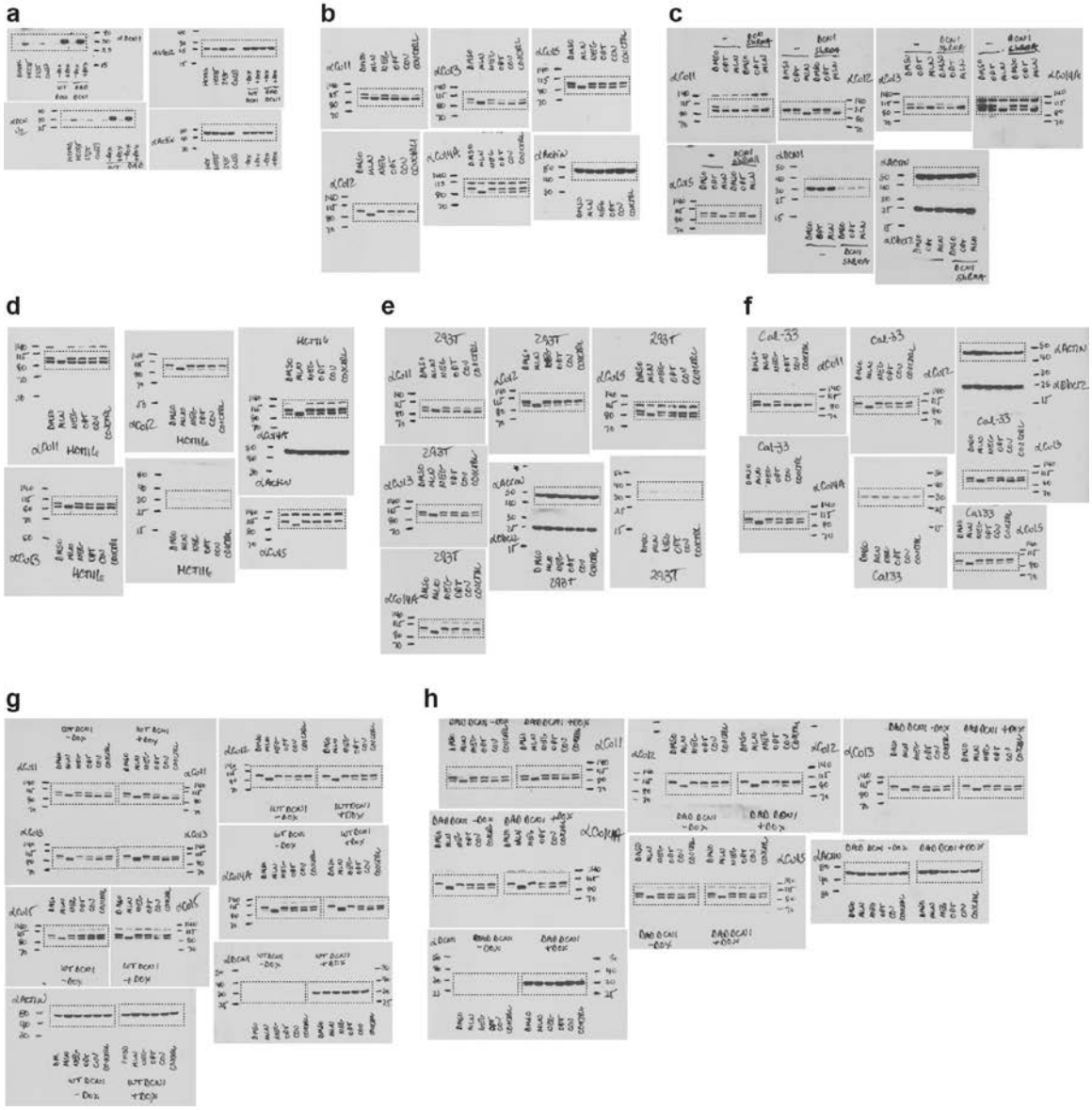

Supplementary Figure 15. Full Gel images for **a.** Figure 5a **b**. Figure 5b **c**. Figure 5c **d.** Figure 5d HCT116 **e**. Figure 5d 293T **f.** Figure 5d CAL-33 **g.** Figure 5d WT DCN1 293T Flp-In **h**. Figure 5d DAD DCN1 293T Flp-In

Supplementary Figure 16

a

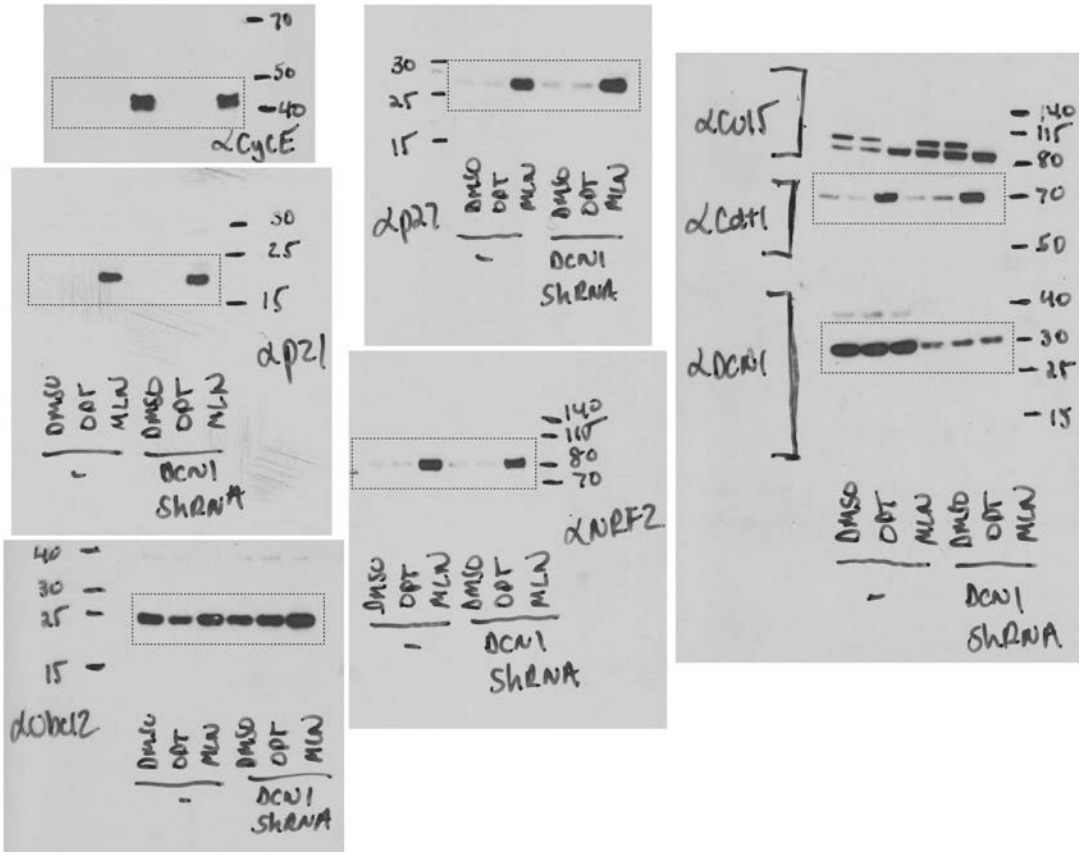

Supplementary Figure 16. Full Gel images for **a.** Figure 6a.

Supplemental Note: Synthetic Information. Synthetic procedures and structural characterization of compounds described in the main text and supplemental information.

Supplemental Dataset 1: Hit Validation Set. Hits from HTS profiled in dose-response format.

Supplemental Dataset 2: Related Analogs. List of >300 compounds contained within our screening collection related to NAcM-HIT profiled in single point or dose-response TR-FRET assay.

Supplemental Dataset 3: Histone Acetyltransferase Off Target Profiling. Raw data for the off target profiling of NAcM inhibitors towards histone acetyltransferases. Experiments were conducted by Reaction Biology. Source data for generating Supplementary Fig 9b.

Supplemental Dataset 4: Bromodomain Off Target Profiling. Raw data for the off target profiling of NAcM inhibitors towards bromodomains. Experiments were conducted by Discover X. Source data for generating Supplementary Fig 9b.

Supplemental Dataset 5: Histone Deacetylase and Sirtuin Off Target Profiling. Raw data for the off target profiling of NAcM inhibitors towards histone deacetylases and sirtuins. Experiments were conducted by Reaction Biology. Source data for generating Supplementary Fig 9b.

Supplemental Dataset 6: UBE2M TMT interaction proteomics. Raw and normalized data for UBE2M IP/MS TMT proteomics in the absence or presence of NAcM-OPT. Source data for generating Fig 4b.

Supplemental Dataset 7: TMT total Proteome data. 8-plex TMT-LC/LC-MS/MS analysis of N-terminal acetylated peptides. List of N-terminal acetylated peptide sequences, protein entries, protein annotation, gene names and the summarized intensities of the TMT reporter ions in 8 channels. Source data for the generating Supplementary Fig11b-f.

Supplemental Dataset 8: Raw data for TMT total proteomics in the absence or presence of NAcM inhibitors. Source data for generating Fig 6b.